Extramitochondrial domain rich in carbonic anhydrase activity improves myocardial energetics

Marie A. Schroeder[a], Mohammad A. Ali[a], Alzbeta Hulikova[a], Claudiu T. Supuran[b], Kieran Clarke[a], Richard D. Vaughan-Jones[a], Damian J. Tyler[a], and Pawel Swietach[a,1]

[a]Burdon Sanderson Cardiac Science Centre, Department of Physiology, Anatomy and Genetics, University of Oxford, Oxford OX1 3PT, United Kingdom; and [b]Dipartimento di Scienze farmaceutiche, Università degli Studi di Firenze, 50019 Florence, Italy

Edited by Robert E. Forster, University of Pennsylvania, Philadelphia, PA, and approved January 16, 2013 (received for review August 10, 2012)

CO_2 is produced abundantly by cardiac mitochondria. Thus an efficient means for its venting is required to support metabolism. Carbonic anhydrase (CA) enzymes, expressed at various sites in ventricular myocytes, may affect mitochondrial CO_2 clearance by catalyzing CO_2 hydration (to H^+ and HCO_3^-), thereby changing the gradient for CO_2 venting. Using fluorescent dyes to measure changes in pH arising from the intracellular hydration of extracellularly supplied CO_2, overall CA activity in the cytoplasm of isolated ventricular myocytes was found to be modest (2.7-fold above spontaneous kinetics). Experiments on ventricular mitochondria demonstrated negligible intramitochondrial CA activity. CA activity was also investigated in intact hearts by ^{13}C magnetic resonance spectroscopy from the rate of $H^{13}CO_3^-$ production from $^{13}CO_2$ released specifically from mitochondria by pyruvate dehydrogenase-mediated metabolism of hyperpolarized [1-^{13}C]pyruvate. CA activity measured upon [1-^{13}C]pyruvate infusion was fourfold higher than the cytoplasm-averaged value. A fluorescent CA ligand colocalized with a mitochondrial marker, indicating that mitochondria are near a CA-rich domain. Based on immunoreactivity, this domain comprises the nominally cytoplasmic CA isoform CAII and sarcoplasmic reticulum-associated CAXIV. Inhibition of extramitochondrial CA activity acidified the matrix (as determined by fluorescence measurements in permeabilized myocytes and isolated mitochondria), impaired cardiac energetics (indexed by the phosphocreatine-to-ATP ratio measured by ^{31}P magnetic resonance spectroscopy of perfused hearts), and reduced contractility (as measured from the pressure developed in perfused hearts). These data provide evidence for a functional domain of high CA activity around mitochondria to support CO_2 venting, particularly during elevated and fluctuating respiratory activity. Aberrant distribution of CA activity therefore may reduce the heart's energetic efficiency.

imaging | pH regulation

Cardiac ventricular myocytes express several carbonic anhydrase (CA) isoforms, which reside in the cytosol (CAII), mitochondria (CAV), sarcolemma (CAIV, CAXIV) and sarcoplasmic reticulum (SR) membrane (CAIV, CAIX, CAXIV) (1, 2). By catalyzing CO_2 hydration and the reverse reaction between H^+ and HCO_3^- ions, these enzymes help to keep CO_2, HCO_3^- and H^+ at chemical equilibrium (3). CA catalysis has been proposed to facilitate transmembrane H^+ and HCO_3^- fluxes responsible for regulating intracellular pH (pH_i) (4–6). The interaction between CA and a membrane-bound transporter has been dubbed the "transport metabolon," although its physiological importance remains contentious (7). For example, transmembrane H^+/HCO_3^- fluxes near resting pH_i may be too small to require CA activity.

A more substantial flux of CA substrate in the heart is mitochondrial CO_2 production by the tricarboxylic acid cycle and the enzyme complex pyruvate dehydrogenase (PDH). Under resting conditions, the heart emits ~3 mmol CO_2 $L^{-1}\cdot min^{-1}$ (based on a myocardial O_2 consumption of 0.1 $mL\cdot min^{-1}\cdot g^{-1}$), and this rate can rise several-fold with increased workload. Locally, at the level of individual mitochondria, CO_2 production fluctuates as a result of oscillating mitochondrial activity (8) regulated by Ca^{2+} transients (9–11) and redox state (12, 13). CO_2 vents out of the mitochondrial matrix, across the cytoplasm, and into the extracellular space, crossing at least three membranes (including two mitochondrial membranes plus the sarcolemma) and a distance of several microns which varies as a result of heterogeneous (14) and time-dependent capillary perfusion (15). This distance includes myoplasm that, because of macromolecular hindrance (16–18), particularly in the radial direction (19, 20), moderately restricts CO_2 diffusion. Mitochondrial membranes (21), like many other membranes (but with exceptions; see ref. 22), are significantly more permeable to CO_2 than to H^+ or HCO_3^- ions, particularly when enriched with gas channels (23). The transmembrane [CO_2] gradient therefore is critical in determining mitochondrial CO_2 efflux. CO_2 venting could be supported by CA-catalyzed buffering of extramitochondrial CO_2 (24), particularly when local CO_2 production is elevated and fluctuating.

The activity of extracellular-facing CA isoforms has been shown to accelerate CO_2 exchange between the intra- and extracellular compartments in the heart (25). However, it has yet to be determined whether CO_2 transport from the matrix to the cytoplasm is facilitated by a particular distribution of CA activity. Previous studies have demonstrated modest CA activity in the cytoplasm (2.6-fold acceleration of CO_2 hydration) (3) and negligible CA activity in mitochondria (26). Such a distribution of CA activity could facilitate CO_2 venting from mitochondria and increase the mitochondrial membrane pH gradient (a component of the proton motive force and a driving force for H^+-coupled solute transport across the inner membrane) (27). A possible link between CA and respiration may be important in cardiac diseases that involve a change in CA isoform expression or activity, such as phenylephrine-induced hypertrophy (28) or dilated cardiomyopathy (29).

We hypothesize that CA activity near (but not within) mitochondria facilitates CO_2 venting and improves myocardial energetics. The distribution of CA activity was investigated using two different approaches to measuring CA catalysis. In the first, pH-sensitive fluorescent dyes assayed cytoplasm-averaged CA activity evoked by rapid CO_2 entry across the sarcolemma (3). In the second, magnetic resonance spectroscopy (MRS) measured CA-catalyzed hydration of $^{13}CO_2$ released by PDH-mediated mitochondrial decarboxylation of the high-signal MRS tracer, hyperpolarized [1-^{13}C]pyruvate (30–32). The effects of CA

Author contributions: M.A.S., A.H., D.J.T., and P.S. designed research; M.A.S., M.A.A., A.H., D.J.T., and P.S. performed research; C.T.S. and K.C. contributed new reagents/analytic tools; M.A.S., M.A.A., A.H., D.J.T., and P.S. analyzed data; and M.A.S., A.H., R.D.V.-J., D.J.T., and P.S. wrote the paper.

Conflict of interest statement: D.J.T. and K.C. received research support from GE Healthcare.

This article is a PNAS Direct Submission.

Freely available online through the PNAS open access option.

[1]To whom correspondence should be addressed. E-mail: pawel.swietach@dpag.ox.ac.uk.

See Author Summary on page 3729 (volume 110, number 10).

This article contains supporting information online at www.pnas.org/lookup/suppl/doi:10.1073/pnas.1213471110/-/DCSupplemental.

activity on energetics were then studied in terms of mitochondrial matrix pH (by fluorescence) and high-energy phosphate metabolites (by ^{31}P MRS). We demonstrate that an extramitochondrial CA domain is an important component of mitochondrial function in the heart, with a capacity to enhance myocardiac energetics.

Results

Ventricular Mitochondria Have Negligible Carbonic Anhydrase Activity. Mitochondrial CA activity was investigated in intact and lysed ventricular mitochondria and in ventricular myocytes subjected to saponin permeabilization, which restricts activity measurements to the mitochondrial compartment. Activity was determined from the rate of acidification after the addition of CO_2-containing solution.

Percoll-purified rat ventricular mitochondria (33) (tested for viability; Fig. S1) were lysed in mitochondrial lysate buffer (MLB), and the medium pH was measured at 4 °C using a Hamilton pH electrode. The CA-catalyzed reaction was triggered by adding CO_2-saturated water (1:2 vol/vol; Fig. 1*A*). A kinetic model described in *SI Computational Methods* was used to best-fit the experimental time courses with a CO_2 hydration constant (k_h) (34). Spontaneous k_h was determined in the presence of the potent CA inhibitor acetazolamide (ATZ) (Fig. S2*A*). CA activity was expressed as a ratio of catalyzed-to-spontaneous k_h. In mitochondrial lysates, CA activity was 1.31 ± 0.11 per mg of total protein. For comparison, CA activity in whole-heart lysates was 2.71 ± 0.08 per mg of total protein, that is, 5.5-fold [(2.71–1)/(1.31–1)] greater than in mitochondrial lysates.

Measurements on mitochondrial lysates may report CA activity with intra- or extramitochondrial catalytic sites. To measure matrix-facing CA activity only, suspensions of intact mitochondria in mitochondrial storage buffer (MSB) were loaded with the membrane-permeant acetoxymethyl (AM) ester of the ratiometric pH-sensitive fluorescent dye BCECF [2′,7′-bis-(2-carboxyethyl)-5-(and-6)-carboxyfluorescein]. After dye loading, mitochondria were washed in dye-free solution to ensure that BCECF reported matrix pH. Upon addition of CO_2-saturated buffer, BCECF reported a fall in pH arising from CO_2 hydration in the matrix. ATZ [permeable across mitochondrial membranes (26)] did not affect pH_i time courses, indicating negligible matrix CA activity. In contrast, the rapid rate of intracellular acidification measured in BCECF-loaded human red cells (positive control for CA activity) was inhibited by ATZ (Fig. S3*A*).

To study mitochondrial CA activity in the native environment of the myocyte, cells were loaded with the ratiometric pH dye cSNARF-1 [5-(and-6)-Carboxy SNARF-1] for 40 min (ensuring adequate mitochondrial dye loading) and then permeabilized by brief (15-s) exposure to 0.005% saponin in Hepes-buffered internal solution (IS). Permeabilization releases cytoplasmic cSNARF-1, and the residual dye reports matrix pH. Exposure to CO_2/HCO_3^--buffered IS reduced matrix pH, resulting from CO_2 influx and hydration, followed by the attainment of a new steady state (Fig. 1 *C*, *i*). ATZ did not reduce the initial slope, adding to the evidence for negligible intramitochondrial CA activity (Fig. 1 *C*, *ii*).

Cytoplasm of Ventricular Myocytes Has Modest CA Activity. CA activity in the cytoplasm of ventricular myocytes was measured from the rate of H^+ production triggered by a rise in intracellular [CO_2]. CO_2 was introduced into isolated myocytes (under continuous superfusion at 37 °C) by switching from Hepes-buffered normal Tyrode (NT) to CO_2/HCO_3^--buffered NT. The progress of the intracellular CA-catalyzed reaction was measured using cSNARF-1 fluorescence (Fig. 2*A*). Dye loading was restricted to 10 min to minimize partitioning into organelles. The degree of subcellular sequestration of cSNARF-1 was determined at the end of each experiment by permeabilizing myocytes with saponin. Upon permeabilization, cSNARF-1 fluorescence (interpolated to the isosbestic wavelength of 605 nm) decreased by 83 ± 2%, indicating that the fluorescence signal in intact myocytes was predominantly cytosolic. The rate of pH_i change upon CO_2 entry (or exit) is a quantitative measure of CA activity (Fig. S3*D*). Because pH_i was acquired over the entire cell, this experimental protocol measured cytosol-averaged CA activity. Using a computational model (34), described in *SI Computational Methods*, k_h was determined to be 0.58 ± 0.08/s and 0.58 ± 0.12/s upon the addition and subsequent removal of CO_2, respectively (n = 17). The measured pH_i changes were not rate-limited by the much faster extracellular solution exchange rate (Fig. S3*B*), and the rate constants obtained were not at the upper limit of the method's resolving power (Fig. S3*C*). Transient exposure to CO_2/HCO_3^- was repeated in the presence of ATZ (100 μM) to measure spontaneous kinetics (0.20 ± 0.02/s and 0.23 ± 0.02/s on CO_2

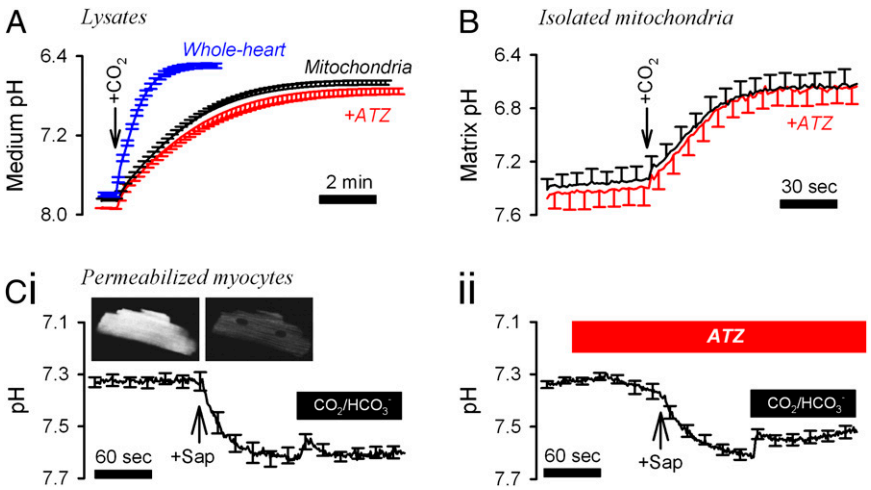

Fig. 1. CA activity in intact and lysed mitochondria. (*A*) CA activity measured by the rate of medium acidification upon the addition of 0.33 mL CO_2-saturated water at 4 °C to a 0.67-mL suspension of mitochondrial or whole-heart lysates prepared in MLB (n = 5 each). Spontaneous kinetics was determined in the presence of the broad-spectrum CA inhibitor ATZ (100 μM). (*B*) Matrix pH of intact mitochondria suspended in MSB, measured using BCECF at room temperature (n = 6). The addition of CO_2-saturated MSB (1:4 vol/vol) acidified the matrix by CO_2 hydration. The experiment was repeated in the presence of ATZ (100 μM). (*C*) (*i*) Ventricular myocytes (n = 8) were superfused at 37 °C with Hepes-buffered IS, permeabilized by means of 15-s treatment with 0.005% saponin (Sap) and then superfused with CO_2/HCO_3^--buffered IS. (*ii*) Experiments were repeated in 100 μM ATZ (n = 9).

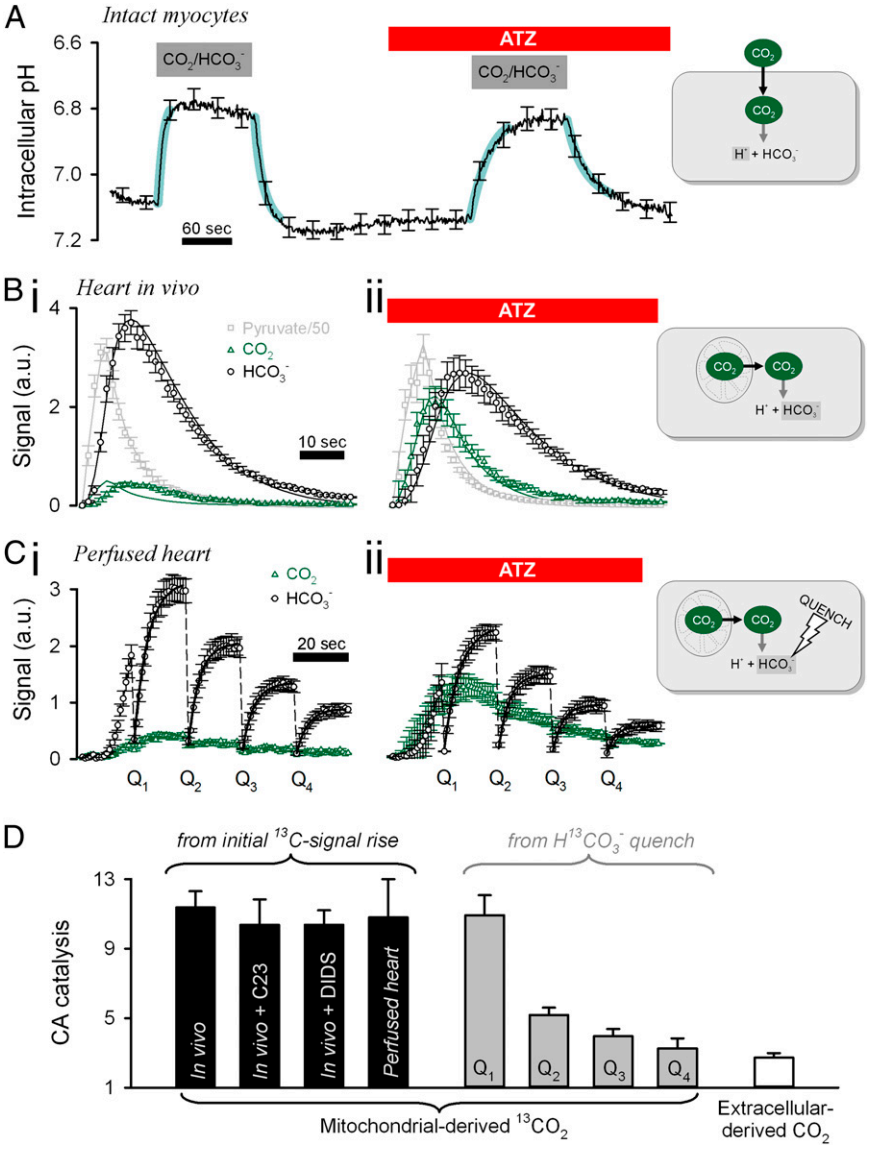

Fig. 2. Intracellular CA activity is concentrated near mitochondria. (*A*) Measuring CA activity in isolated, intact myocytes (n = 17) under superfusion at 37 °C. Switching from Hepes-buffered NT to CO_2/HCO_3^--buffered NT (and back) evokes a pH_i change proportional to the intracellular CA activity. The experiment was repeated in the presence of the CA inhibitor ATZ (100 μM). Thick cyan lines show best-fit simulation (CA activity of 2.7). (*B*) Measuring cardiac CA activity in rats infused in vivo with metabolic tracer. (*i*) Time course of ^{13}C-labeled pyruvate, CO_2, and HCO_3^- measured by MRS of rats infused with 80 μmol of hyperpolarized [1-^{13}C]pyruvate (n = 8). (*ii*) The experiment was repeated on rats pretreated with 25 μmol ATZ 15 min before the infusion of [1-^{13}C]pyruvate (n = 6). Continuous traces show the best-fit model simulation (CA activity 11.4). (*C*) Measuring cardiac CA activity in Langendorff-perfused rat hearts. Hearts were perfused with 0.6 mM [1-^{13}C]pyruvate, and ^{13}C-labeled metabolites were measured by MRS (n = 5); the experiment was repeated with 100 μM ATZ (n = 5). For clarity, only $^{13}CO_2$ and $H^{13}CO_3^-$ time courses are shown. The [1-^{13}C]pyruvate signal attained a peak at ~30 s. The $H^{13}CO_3^-$ signal was quenched (Q_1–Q_4) every 20 s to trigger $^{13}CO_2$ hydration. The initial rate of $H^{13}CO_3^-$ reappearance was obtained from exponential best-fit. (*D*) Apparent CA activity measured under different experimental protocols. Black bars: From the initial appearance of $H^{13}CO_3^-$-signal. Membrane-impermeable CA inhibitor C23 was infused at 2 μmol, and the Cl^-/HCO_3^- exchange inhibitor DIDS (n = 3) was infused at 25 μmol to rats in vivo; control experiments were repeated on Langendorff-perfused hearts ex vivo (n = 8). Gray bars: After sequential $H^{13}CO_3^-$-quenching reactions, once every 20 s. White bar: Upon addition of CO_2 from the superfusate.

addition and removal, respectively), which were in agreement with uncatalyzed kinetics (35, 36). Thus, CA activity across the cytosol accelerated CO_2 hydration by a factor of 2.7 ± 0.3.

Ventricular Mitochondria Are Close to a Domain Rich in CA Activity. In an alternative approach to measuring CA activity, CO_2 was introduced into the cytoplasm by mitochondrial decarboxylation of pyruvate. This process and the subsequent CO_2 hydration to HCO_3^- was measured using ^{13}C MRS following the administration of [1-^{13}C]pyruvate to intact hearts. To improve the signal-to-noise ratio of measurements, ^{13}C-labeled pyruvate was subjected to a hyperpolarization procedure (30). Labeling the first carbon of pyruvate ensured that the source of $^{13}CO_2$ was exclusively the mitochondrial activity of PDH (32, 37). Thus, CA activity could be measured locally in the $^{13}CO_2$-containing cell domain by the rate of $H^{13}CO_3^-$ production.

The hyperpolarized metabolic tracer [1-^{13}C]pyruvate was infused i.v. into anesthetized living rats, and ^{13}C spectra were acquired from a surface coil placed over the rat's chest to detect PDH activity predominantly from the heart (32). Fig. 2 *B*, *i* shows the average time courses of ^{13}C-labeled compounds measured by MRS. Experiments also were performed on animals pretreated with 25 μmol

ATZ (Fig. 2 *B*, *ii*) or 2 μmol of the membrane-impermeant CA inhibitor C23 [4-(2,4,6-trimethylpyridinium-*N*-methylcarboxamido)-benzenesulfonamide perchlorate] (Fig. S2*B*) (38). The initial rate of $H^{13}CO_3^-$ production measures CO_2 hydration near its site of production. ATZ reduced the initial slope and the peak of the $H^{13}CO_3^-$ signal (normalized to peak [1-^{13}C]pyruvate) by 85% and 24%, respectively, and increased the initial slope and the peak of the $^{13}CO_2$ signal by 70% and 88%, respectively. In contrast, C23 had no effect on the ^{13}C time courses (Fig. S3*E*). Because the mitochondrial matrix has no detectable CA activity (Fig. 1), the effect of ATZ must arise from the activity of extramitochondrial CA enzymes.

The CO_2 hydration constant k_h, ^{13}C signal decay, and PDH activity were determined by best-fitting to a computational simulation (Fig. S3*F*), as described in *SI Computational Methods* (31). ATZ and C23 had no effect on PDH activity itself (0.0049 ± 0.0004, 0.0043 ± 0.0006, and 0.0051 ± 0.0005/s in ATZ, C23, and control, respectively) or on the signal-decay constant of either [1-^{13}C]pyruvate (0.14 ± 0.01, 0.13 ± 0.02, and 0.16 ± 0.01/s, respectively) or $^{13}CO_2/H^{13}CO_3^-$ (0.091 ± 0.08, 0.084 ± 0.04, and 0.073 ± 0.01/s, respectively). The best-fit k_h was 2.2 ± 0.2/s under control conditions and 0.19 ± 0.01/s in the presence of ATZ. Thus, CA activity accelerated CO_2 hydration in the $^{13}CO_2$-rich domain by a factor of 11.4 ± 0.9. This measurement of CA activity within a spatially confined region of the cell was considerably higher than the cytosol-averaged estimate (Fig. 2*A*) matched for pH_i, and temperature. C23 did not affect k_h (2.1 ± 0.2/s), confirming that the method was assaying intracellular CA activity only (Fig. S3*E*). These data suggest that a cytoplasmic domain near mitochondria is enriched in CA activity.

In the in vivo experiments described above, CAII activity in red cells could be affecting the CA activity measurements. To test this possibility, experiments were performed on rats infused with 25 μmol DIDS (4,4′-diisothiocyanatostilbene-2,2′-disulfonic acid) to block HCO_3^- exchange between red cells and plasma and, in separate experiments, on Langendorff-mode Krebs–Henseleit buffer (KHB)–perfused hearts ex vivo. The best-fit k_h (in vivo with DIDS: 2.0 ± 0.3/s; ex vivo: 2.0 ± 0.2/s) was not different from measurements on control hearts in vivo, arguing against a contribution from red cell CA. Results from Langendorff-perfused hearts also confirm that the ^{13}C time courses measured in rats in vivo were cardiac in origin.

The ^{13}C-based method described so far inferred CA activity from the initial rate of appearance of hyperpolarized $H^{13}CO_3^-$ and $^{13}CO_2$ signals. CA activity was probed further using an alternative ^{13}C-based protocol involving $H^{13}CO_3^-$-signal quenching to drive CO_2/HCO_3^- out of equilibrium. A radio-frequency electromagnetic pulse was applied every 20 s after the administration of hyperpolarized [1-^{13}C]pyruvate to Langendorff-perfused hearts. Each quenching pulse permanently destroyed all MR signal originating from the hyperpolarized $H^{13}CO_3^-$ pool without directly affecting the $^{13}CO_2$ signal. The rate of $H^{13}CO_3^-$ production after each quench therefore measures the current $^{13}CO_2$ hydration rate (Fig. 2 *C*, *i*). This was quantified from the initial slope of the $H^{13}CO_3^-$ signal increase divided by the $^{13}CO_2$ signal amplitude and normalized to measurements from ATZ-treated hearts (100 μM; n = 5) (Fig. 2 *C*, *ii*). After the first quenching reaction (Q_1), CA activity (10.9 ± 1.2; control k_h = 2.12 ± 0.22/s; ATZ k_h = 0.19 ± 0.01/s) was similar to that determined from the initial appearance of the $H^{13}CO_3^-$ signal (Fig. 2*B*). However, subsequent quenching reactions yielded a lower CA activity (Fig. 2*D*), suggesting that the distribution of $^{13}CO_2$ signal had changed with time to a spatial domain encompassing a lower CA density. Because hyperpolarized $^{13}CO_2$ is washed out of the perfused heart, the amplitude of its global signal declines, as observed experimentally (Fig. 2*C*). During this washout period, which lasts for tens of seconds, much of the remaining hyperpolarized $^{13}CO_2$ permeates into neighboring and down-stream myocytes and there, it undergoes hydration to $H^{13}CO_3^-$, catalyzed by bulk cytoplasmic CA. Meanwhile, de novo $^{13}CO_2$ signal production by mitochondria decreases because of spin-lattice relaxation of hyperpolarized [1-^{13}C] pyruvate [decaying to 1/e of its original value in 50–60 s (31)]. Therefore it is notable that spatial dispersal of the myocardial $^{13}CO_2$ signal was associated with a shift in the measured CA activity from the high initial value associated locally with mitochondria to a more modest value typical of that measured previously in superfused myocytes, when CO_2 was delivered exogenously to bulk cytoplasm (Fig. 2*A*). Thus, depending on the time period after acute introduction of hyperpolarized [1-^{13}C]pyruvate to the perfused heart, the $H^{13}CO_3^-$-quenching protocol provides estimates of CA activity that are consistent initially with a high local, extramitochondrial value and subsequently with a lower more general cytoplasmic value.

Fluorescent CA Ligand Colocalizes with Mitochondria. Cytosol-facing CA catalytic sites were visualized in permeabilized myocytes bathed in mitochondrial respiration buffer (MRB) using the fluorescein-conjugated CA inhibitor (F-CAI) (38). After 90-s exposure to the ligand (1 mM), unbound F-CAI was washed out by superfusion. Compared with the water-soluble derivative fluorescein sulfonate (FS), F-CAI bound more stably to membranes (Fig. S4*A*), so that after 60-s washout, fluorescence was derived mainly from CA-bound F-CAI. A similar procedure was followed for the membrane-tagging derivative DHPE-fluorescein [DHPE-F; N-(fluorescein-5-thiocarbamoyl)-1,2-dihexadecanoyl-sn-glycero-3-phosphoethanolamine triethylammonium] used as a positive control for mitochondrial membrane staining. [NB: Substantially longer (>10 min) dye loading leads to dye accumulation in the intermembrane space.]

Mitochondria were visualized using the fluorescent marker tetramethylrhodamine ethyl (TMRE) loaded before permeabilization. At 488-nm excitation, fluorescein fluorescence bleed-through to the TMRE detection range was only 11% (Fig. S4*B*) and was corrected for in subsequent analyses. Colocalization between TMRE and either F-CAI or DHPE-F was determined by simultaneous imaging after 60-s washout of unbound fluorescein derivative (Fig. 3*A*). The lack of FRET from F-CAI to TMRE indicated that F-CAI did not enter mitochondria (Fig. S4*C*), as expected from its membrane impermeability (38).

Correlation of the fluorescence intensity in the TMRE and fluorescein signals was quantified pixel by pixel and plotted as a binned scatter plot (Fig. S4*D*). Soluble FS and membrane-tagging DHPE-F were used as negative and positive controls, respectively, for mitochondrial colocalization. The high Pearson's correlation coefficient obtained with F-CAI and its reduction in the presence of the nonfluorescent competitor ATZ (Fig. 3*B*) suggested that mitochondria are in close contact with a CA-rich cytosolic domain.

Extramitochondrial CAXIV and CAII Are Detected in Isolated Mitochondria. The identity of CA isoforms associated with the CA-rich extramitochondrial domain was tested by immunoreactivity. Mitochondrial samples were prepared using the Percoll method (39), and several washing steps were applied in an attempt to purify the sample. Mitochondrial samples were then compared with lysates prepared from isolated myocytes. Lactate dehydrogenase B (LDH-B) immunoreactivity, strongly present in total myocyte lysates, diminished to undetectable levels in mitochondrial samples after the first washing step (sample #1). The washing procedure therefore had removed unbound soluble cytosolic proteins (Fig. 3 *C*, *i*). Sample #1 was positive for CAXIV (a membrane-tethered isoform) and CAII (a nominally soluble isoform) (2). The mitochondrial marker mitofilin and matrix CA isoform VA were strongly detected after the second wash (sample #2) and remained after a subsequent wash (sample #3), indicating that a highly enriched mitochondrial sample had been achieved after two rounds of washing. In the process of mitochondrial enrichment (sample #2 vs. #1), CAXIV immunoreactivity increased markedly and then remained stable following subsequent washing steps

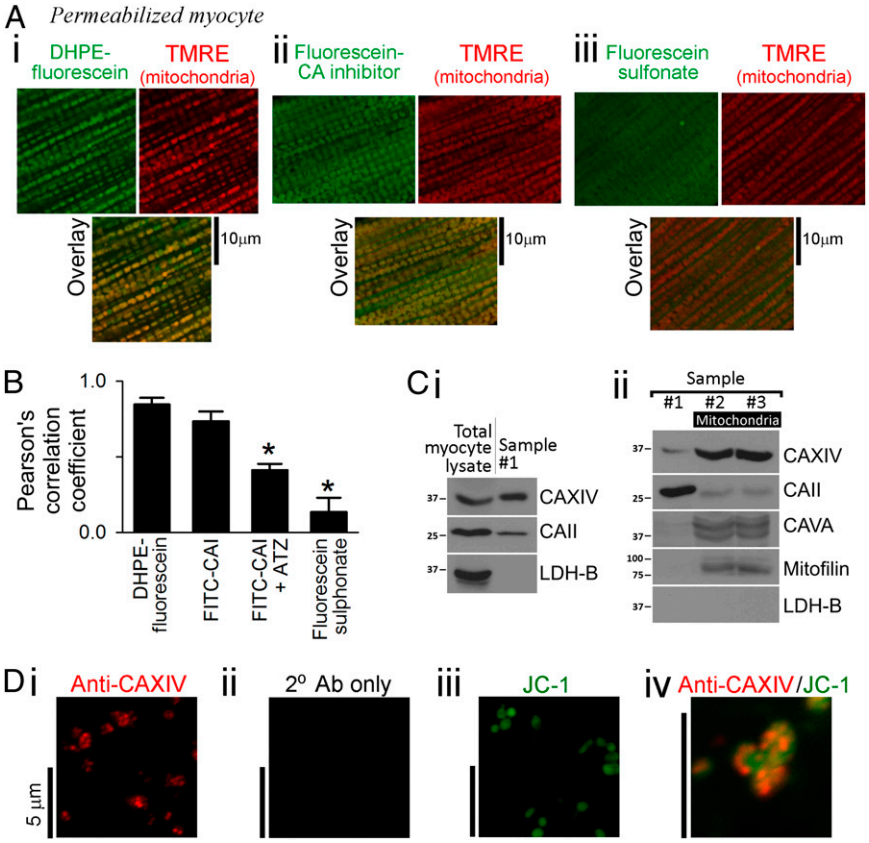

Fig. 3. Mitochondria colocalize with CA enzymes. (*A*) TMRE-loaded myocytes were permeabilized and exposed to one of three fluorescein derivatives (1 mM) for 90 s: (*i*) membrane-tagging DHPE-F; (*ii*) the fluorescent CA inhibitor F-CAI; and (*iii*) FS. Fluorescein (excited at 488 nm) measured <555 nm; TMRE (excited at 555 nm) measured >600 nm. Fluorescence images (100× magnification) were captured after 60 s of washout to remove unbound fluorophores. (*B*) Pearson's correlation coefficients between TMRE and fluorescein derivatives. Correlation with F-CAI was reduced in the presence of the nonfluorescent CA inhibitor ATZ (1 mM). Asterisk denotes significant difference ($P < 0.05$) vs. DHPE-F. (*C*) Western blots were performed on total myocyte lysate, and samples were taken after three consecutive washing steps in the mitochondrial purification procedure. Immunoreactivity was tested for CA isoforms XIV, VA, and CAII, the mitochondrial marker mitofilin, and the cytoplasm marker LDH-B. Samples 2 and 3 are enriched in mitochondria. CAXIV and CAII remain associated with mitochondria. (*D*) Immunofluorescence of mitochondrial sample for (*i*) CAXIV, (*ii*) secondary antibody only (negative control), and (*iii*) mitochondrial marker JC-1; (*iv*) overlay of CAXIV and JC-1 staining.

(sample #3 vs. #2; Fig. 3 *C*, *ii*). The presence of small but consistently measureable CAII immunoreactivity (Fig. 3 *C*, *i*; repeated five times) even after five washing steps (Fig. S5*A*) suggests that some of this cytosolic protein associates with mitochondria. Mitochondrial samples showed immunoreactivity to sarcoplasmic reticulum Ca^{2+} ATPase 2a (SERCA2A) but not ryanodine receptor type 2 (RyR2) (Fig. S5*B*), suggesting that the presence of CAXIV protein in isolated mitochondria may arise from their interaction with network (rather than junctional) SR (40). The colocalization of CAXIV immunoreactivity with mitochondria was tested with immunofluorescence. CAXIV staining was concentrated within particles of regular size (diameter 0.5–1.0 μm; Fig. 3 *D*, *i*) expected of mitochondria (Fig. 3 *D*, *iii*). Furthermore, colocalization was observed in samples stained dually for CAXIV and the mitochondrial indicator JC-1 (5,5′,6,6′-tetrachloro-1,1′,3,3′-tetraethylbenzimidazolylcarbocyanine iodide; Fig. 3 *D*, *iv*).

Extramitochondrial CA Activity Raises Mitochondrial Matrix pH but Not Cytoplasmic pH. The presence of an extramitochondrial CA-rich domain may affect mitochondrial matrix pH by facilitating CO_2 venting (7, 24). This possibility was studied by measuring pH in myocytes that had been saponin-permeabilized and superfused (37 °C) with mitochondrial respiration buffer (MRB) at pH 7.15 (Fig. 4*A*). Fluorescence from cSNARF-1–loaded permeabilized myocytes reports ensemble matrix pH. In the presence of 5 mM ATP, 80 μM ADP, and mitochondrial substrates to stimulate respiration (41), the matrix was found to acidify in response to CA inhibition with 100 μM ATZ. This effect was not associated with any significant change in mitochondrial membrane potential ($\Delta\psi$) measured using JC-1 (Fig. S6). In myocytes preincubated with ATZ for 30 min before permeabilization, steady-state matrix pH was 0.11 units lower than in untreated cells.

In separate experiments, pH was measured ratiometrically using fluorescein derivatives, which target different compartments of the cell. DHPE-F applied to permeabilized cells for 10 min concentrates in the intermembrane space (IMS) (42), as validated by the pH response to carbonyl cyanide-4-(trifluoromethoxy) phenylhydrazone (FCCP) and electron transport chain inhibitors (Fig. S7*A*). Following a similar loading procedure, wheat germ agglutinin-conjugated fluorescein (WGA-F) binds to the partially disrupted sarcolemmal and T-system and the nucleus, further away from mitochondria (Fig. S7 *B*, *ii*). Bulk solution pH was reduced to 7.0 to improve the sensitivity of fluorescein signal to changes in pH. It was necessary to stimulate respiration with 300 μM ADP to resolve the potentially small changes in pH measured with WGA-F and DHPE-F. Although the pH reported by WGA-F was close to bulk pH, DHPE-F measured a more acidic level, consistent with its targeting to the IMS. Upon CA inhibition with ATZ, DHPE-F, but not WGA-F, reported a decrease in pH (by 0.04 pH units; Fig. 4 *A*, *i*), suggesting that the site of CA activity is between the IMS and the bulk cytoplasm.

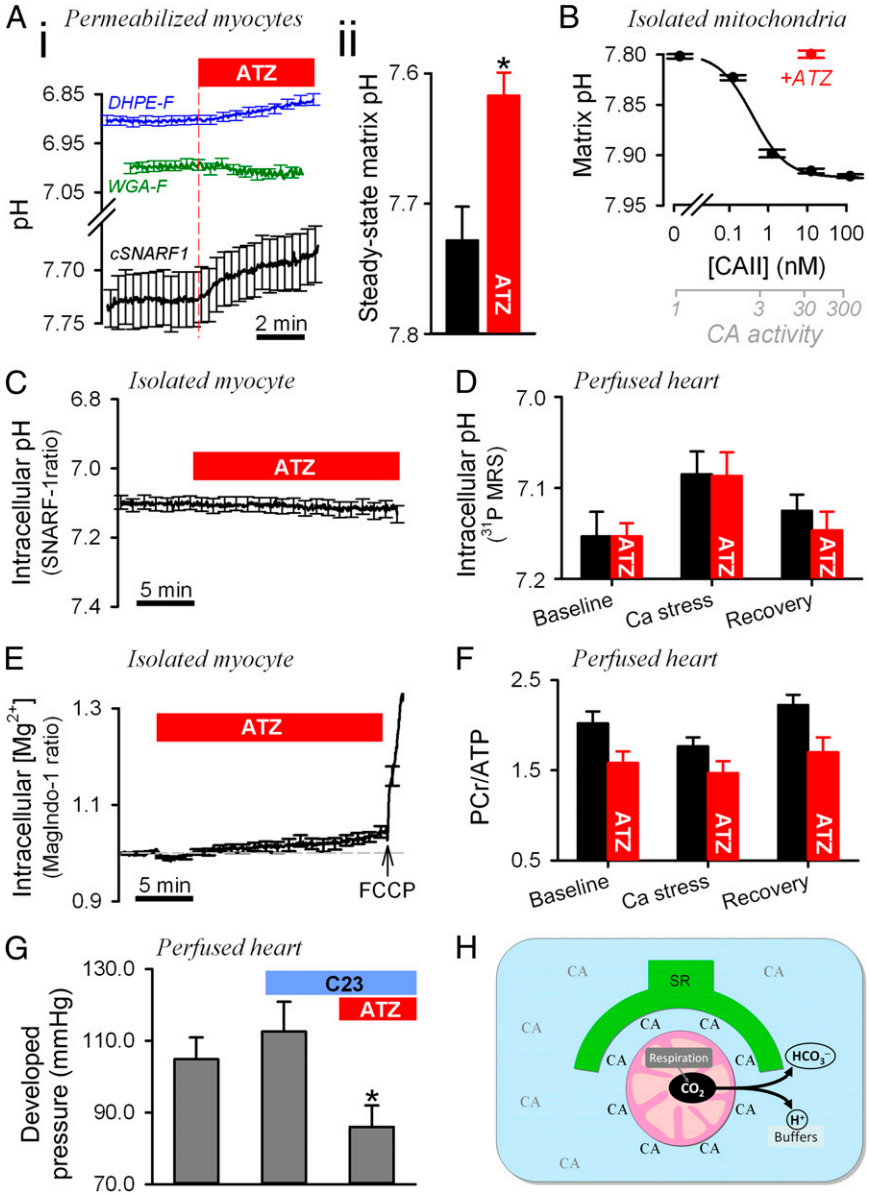

Fig. 4. Effect of CA activity on mitochondrial pH, cytoplasmic pH, energetics, and contractility. (*A*) Experiments on saponin-permeabilized ventricular myocytes superfused in MRB. (*i*) Effect of ATZ (100 μM) on pH measured with membrane-tagging DHPE-F (reporting pH in intermembrane space; $n = 34$; blue trace), glycoprotein-binding WGA-fluorescein (reporting pH near sarcolemma and T system; $n = 28$; green trace), and cSNARF-1 (reporting pH in matrix; $n = 31$; black trace). To stimulate respiration, experiments with DHPE-F and WGA-F were performed using higher (300 μM) ADP. Significant acidification ($P < 0.01$) was recorded with cSNARF-1 and DHPE-F. (*ii*) Steady-state matrix pH in myocytes pretreated with 100 μM ATZ for 30 min before permeabilization ($n = 25$) vs. control ($n = 41$) ($P = 0.007$). (*B*) Relationship between exogenously supplied extramitochondrial CAII and matrix pH in suspensions of cSNARF-1–loaded mitochondria in state III respiration. Best-fit to Hill curve. Experiments with 10 nM CAII were repeated with 100 μM ATZ. Error bars show coefficient of variation. ($n = 6$–10 repeats/dose.) (*C*) Effect of ATZ (100 μM) on cytoplasmic pH measured in cSNARF-1–loaded myocytes superfused with CO_2/HCO_3^--buffered NT containing 2 mM pyruvate ($n = 25$). (*D*) Cytoplasmic pH measured in perfused hearts by ^{31}P MRS under baseline conditions at the end of 15-min Ca^{2+} stress (double perfusate [Ca^{2+}]) and upon recovery ($n = 8$). Experiments were repeated with 100 μM ATZ ($n = 8$). Two-way ANOVA: $P = 0.008$ for Ca^{2+} stress; $P = 0.68$ for ATZ. (*E*) Effect of ATZ (100 μM) on Mag-Indo-1 fluorescence ratio measured in myocytes ($n = 20$) superfused with CO_2/HCO_3^--buffered NT containing 2 mM pyruvate. The effect of FCCP (1 μM) confirmed the inverse $[Mg^{2+}]_i$–$[ATP]_i$ relationship. (*F*) PCr/ATP ratio measured in perfused hearts ($n = 4$ control, $n = 6$ with ATZ) using ^{31}P MRS. Two-way ANOVA for ATZ: $P = 0.009$. (*G*) Developed pressure in the left ventricle of perfused hearts sequentially exposed to 35 μM C23 (not significant) and 100 μM ATZ plus 35 μM C23 ($P = 0.01$). (*H*) Cartoon showing the CA-rich domain near mitochondria and its role in facilitating CO_2 venting from the matrix. Extramitochondrial CA enzymes include cytoplasmic and SR-associated isoforms.

Inhibition of CA activity therefore leads to the accumulation of acid in the matrix and, to a lesser extent, in the IMS.

The effect of ATZ on matrix pH was studied further by flow cytometry of isolated, cSNARF-1–loaded mitochondria at room temperature (Fig. S8*A*). Mitochondria were incubated under state III respiration (i.e., ADP stimulated, with excess substrate) to enhance CO_2 production. Extramitochondrial CA activity was varied experimentally by adding up to 250 nM bovine red cell CAII. CA activity in these suspensions was determined in separate experiments from the rate of medium acidification upon the addition of CO_2-saturated water. CO_2 hydration was accelerated 84% per nanomolar CAII at 4 °C (Fig. S8*B*). Based on the enzyme's temperature sensitivity (35), CAII activity increases CO_2 hydration 313%/nM at 25 °C. CAII at 3.2 nM produced

a milieu that accelerated CO_2 hydration 11-fold, i.e., the level measured in the intact extramitochondrial domain of myocytes (Fig. 2*B*). Raising extramitochondrial CA activity was found to increase the population-average matrix pH by up to 0.12 units in an ATZ-sensitive manner (Fig. 4*B*). The half-maximal effect was attained with 0.4 nM CAII (equivalent to 2.2-fold CA catalysis). Thus, the extramitochondrial CA activity normally present in intact myocytes would be sufficient to raise matrix pH.

To test for effects of CA activity on resting cytoplasmic pH, intact ventricular myocytes were loaded for 5 min with cSNARF-1 and superfused with CO_2/HCO_3^--buffered NT solution containing 2 mM pyruvate. Permeabilization performed at the end of each experiment confirmed a low (<15%) degree of dye sequestration into mitochondria. Resting cytoplasmic pH was not affected by the addition of 100 μM ATZ, even after 20 min exposure (Fig. 4*C*). Cytoplasmic pH also was measured in Langendorff-perfused hearts by ^{31}P MRS [using the frequency difference between phosphocreatine (PCr) and inorganic phosphate (P_i) peaks]. After 30 min perfusion to attain steady state, cytoplasmic pH was not different in control and hearts treated with 100 μM ATZ (Fig. 4*D*). To test for effects of ATZ during increased workload, positive inotropy was imposed by doubling perfusate [Ca^{2+}] from 1.35 mM to 2.7 mM for 15 min (Ca^{2+} stress). This maneuver reduced cytoplasmic pH, but ATZ had no additional effect.

CA Activity Improves Myocardial Energetics. The effect of CA activity on increasing the pH gradient across the inner mitochondrial membrane (ΔpH) may regulate mitochondrial function by changing the proton motive force (PMF) and the driving force for transport processes such as pyruvate and P_i uptake and Ca^{2+} removal (27). The relationship between CA activity and energetics was investigated in isolated myocytes (superfused with CO_2/HCO_3^--buffered NT containing 2 mM pyruvate) by measuring intracellular [Mg^{2+}] levels, which are inversely related to intracellular [ATP] (43). Exposure to 100 μM ATZ resulted in a decrease followed by a slow recovery and overshoot in free [Mg^{2+}] measured using Mag-Indo-1. However, these changes were less than 4%, suggesting that [ATP] is highly buffered. The impermeant CA inhibitor C23 did not evoke this biphasic pattern of [Mg^{2+}], indicating that the metabolic response was caused by intracellular CA isoforms.

An important buffer that keeps [ATP] nearly constant is the creatine kinase equilibrium involving phosphocreatine (PCr). To assess the state of the heart's energetic reserve, the ratio of PCr to ATP was determined from ^{31}P MR spectra of Langendorff-perfused hearts. The addition of 100 μM ATZ decreased the PCr/ATP ratio significantly (Fig. 4*F*). Given the constancy of ATP and the decrease in PCr/ATP in response to ATZ, the creatine kinase equilibrium predicts a substantial increase in free cytoplasmic [ADP] (44). The overall decrease in free energy available in high-energy phosphates can contribute to impaired contractility (45). Developed pressure (DP) was unaffected in the presence of 35 μM C23 but decreased within 40 min of perfusion in the additional presence of 100 μM ATZ (Fig. 4*G*), indicating that extracellular-facing CA sites do not underlie the observed responses to ATZ. The ATZ effect was not associated with a change in the normalized rate of rise or fall of pressure (dP/dt): $[dP/dt]_{max}/DP$: 21.1 ± 1.3 s^{-1} vs. 21.7 ± 1.4 s^{-1}; $[dP/dt]_{min}/DP$: 17.4 ± 0.9 s^{-1} vs. 17.2 ± 1.0 s^{-1} for C23 and C23+ATZ, respectively.

Discussion

Intracellular Carbonic Anhydrase Activity Is Highly Compartmentalized. The 13 catalytically active CA isoforms are commonly categorized as cytosolic (CAI, II, III, VII and XIII), mitochondrial (VA and VB), secreted (VI), and membrane-associated (IV, IX, XII, XIV, XV). The complex architecture of cardiac myocytes features H^+, HCO_3^-, and CO_2 fluxes at discrete loci, and therefore it is important to understand the distribution of CA activity at fine spatial resolution. This study demonstrates that ventricular mitochondria (a major source of CO_2) have negligible CA activity in their matrix but are surrounded by a domain of high CA activity.

Our finding of negligible intramitochondrial CA activity is in agreement with previous measurements performed on dilute suspensions of broken and intact cardiac mitochondria (26). The protocols used herein (Fig. 1 *B* and *C*) restricted pH recordings to within the mitochondria, eliminating the possibility that excessive dilution of mitochondrial matter is the cause of apparently low CA activity. High CA activity in the extramitochondrial domain was inferred from the observation that the cytoplasm-averaged CO_2 hydration rate (measured using a pH-sensitive dye dissolved in the cytoplasm; Fig. 2*A*) was fourfold lower than the rate of conversion of mitochondrially released $^{13}CO_2$ to $H^{13}CO_3^-$ (Fig. 2*B*). $^{13}CO_2$ production was confined to mitochondria by infusing hearts with [1-^{13}C]pyruvate, a substrate metabolized by pyruvate dehydrogenase to form $^{13}CO_2$ exclusively in the matrix (32, 37). Cytoplasm-averaged CA activity agrees with previous measurements of intracellular CA catalysis (3), but CA activity near mitochondria has not been quantified previously.

Colocalization of a CA-binding fluorescent drug with the mitochondrial marker TMRE suggests that CA catalytic sites are present near mitochondria (Fig. 3*A*). The use of a membrane-impermeant fluorescent CA ligand on surface-permeabilized cells precluded binding to CA sites inside organelles such as in the SR lumen. The extramitochondrial CA-rich domain appears to consist of CAXIV. Levels of this isoform increased during mitochondrial purification (Fig. 3*C*), and immunofluorescence demonstrated its colocalization with mitochondria (Fig. 3*D*). Because CAXIV is present on the network (longitudinal) SR membrane (2), the extramitochondrial CA domain may be constructed on an SR framework. Immunoreactivity for SERCA2a (but not RyR2) in isolated mitochondria (Fig. S5) further supports the mounting evidence for a close structural and functional relationship between mitochondria and specific compartments of the SR (46, 47). Little is known about the specific role of SR-associated CAXIV in tissues. In contrast, CAXIV activity at the surface membrane has been shown to buffer the brain's extracellular space (48), facilitate lactic acid transport in skeletal muscle (49), and enhance Cl^-/HCO_3^- exchange in cardiac myocytes, particularly from hypertrophied hearts (50). Purified samples of mitochondria were consistently positive for CAII immunoreactivity, despite the complete washout of the cytosolic protein LDH-B (Fig. 3*C*). Previous studies have demonstrated CAII binding to the cell membrane (5–7, 51), and a similar interaction may take place with the mitochondrial membranes. An association between CAII/CAXIV and mitochondrial membranes may explain why modest CA activity was detected in mitochondrial lysates (Fig. 1*A*) but not in the matrix of intact mitochondria (Fig. 1*B*). It should be noted that CA activity associated with isolated mitochondria is likely to be lower than in the intact environment of cells because of membrane disruption caused by the isolation procedure.

Extramitochondrial CA Activity Improves the Efficiency of Mitochondrial Respiration. Inhibition of CA activity with ATZ evoked a slow but sustained acidification of the mitochondrial matrix by ~0.1 pH units at steady state (Fig. 4 *A* and *B*). Matrix acidification was associated with a concurrent (albeit smaller) acidification of the intermembrane space (Fig. 4*A*), suggesting that the ATZ effect cannot be explained by the inhibition of the electron transport chain (which would have produced opposite pH effects on either side of the inner membrane). The pH in the bulk cytoplasm (Fig. 4*C*) or near the sarcolemma (Fig. 4*A*) did not acidify in response to ATZ, indicating that the drug targets CA enzymes close to the mitochondrial CO_2 source.

The alkalinizing effect of extramitochondrial CA activity on cell-averaged matrix pH can be explained in terms of facilitated CO_2 venting from mitochondria. The activity of individual mitochondria oscillates and can vary considerably in magnitude (8–

13); therefore CO_2 production will not be in a steady state locally (although the ensemble flux may appear so). Extramitochondrial CA activity can convert $[CO_2]$ changes into relatively much smaller $[HCO_3^-]$ changes (in the presence of pH buffers). This chemical conversion helps maintain a lower $[CO_2]$ at the outer surface of respiring mitochondria, improving mitochondrial $[CO_2]$ venting and shortening the time interval during which matrix $[H^+]$ overshoots, thereby reducing the time-averaged ensemble matrix $[H^+]$. Anchoring CA enzymes in the aqueous compartment near mitochondria, along the path of CO_2 diffusion, increases the available catalytic potential for CO_2 buffering. Extramitochondrial CA activity also may dampen the amplitude of cytoplasmic $[CO_2]$ fluctuations arising from temporal changes in capillary perfusion (14, 15). In summary, by chemically buffering cytoplasmic $[CO_2]$, extramitochondrial CA activity allows a more stable matrix pH and hence ATP production. Extramitochondrial CA activity can be particularly important for matching energy supply with demand. During systole–diastole cycles, changes in cytoplasmic $[Ca^{2+}]$ have been proposed to regulate mitochondrial respiration in order to keep the ATP supply constant (52, 53). This matching would be disrupted if matrix pH were allowed to fall after each systolic rise in energy demand. It is important to note that CA activity inside mitochondria would not achieve the same beneficial effects as extramitochondrial CA, perhaps explaining why mitochondria of metabolically active tissue (such as heart) have no detectable matrix CA activity (26, 54).

The CO_2 diffusion coefficient in cardiac cytoplasm is likely to be reduced by the highly organized network of proteins (16–18), particularly in the radial direction because of anisotropy (19, 20), giving an estimated radial tortuosity factor of three- to 11-fold. CA catalysis has been demonstrated (24) to facilitate CO_2 diffusion in aqueous compartments by allowing a parallel flux of HCO_3^-. However, over the short mitochondria–sarcolemma distances, the modest CA activity measured in cardiac cytoplasm is unlikely to produce a major facilitation of cytoplasmic CO_2 diffusion.

Accelerated CO_2 hydration by extramitochondrial CA may be expected to acidify the cytoplasm, but this acidification was not observed (Fig. 4 *C* and *D*). A likely explanation may be that any changes in cytoplasmic pH are too small to resolve. Mitochondria occupy a third of the cell volume, and their intrinsic buffering capacity is threefold lower than cytoplasmic buffering (55). If CA activity raises matrix pH by 0.1 units, changes in cytoplasmic pH would be below resolving power (~0.01). Additionally, the pH of the cytoplasm is regulated directly by pH-sensing acid/base transporters, such as Na^+/H^+ exchange (56).

The inner membrane pH gradient contributes to the ATP-generating PMF and the driving force for Ca^{2+} extrusion (by Ca^{2+}/H^+ exchange), phosphate uptake (on P_i-H^+ cotransport), and pyruvate uptake (on H^+-monocarboxylate transport) (27). CA inhibition was found to decrease ΔpH without affecting mitochondrial membrane potential (Δψ) (Fig. S6), reiterating the notion that these components of PMF can be regulated independently (27). A decrease in PMF, P_i, and pyruvate uptake is predicted to decrease ATP production, whereas matrix Ca^{2+} accumulation would stimulate respiration (27, 52, 53). Measurements of $[Mg^{2+}]_i$, an inverse indicator of $[ATP]_i$, suggested that CA inhibition did not change ATP levels by more than 4% (Fig. 4*E*). However, the small but reproducible biphasic $[Mg^{2+}]$ time course suggests that the cell had undergone changes in its energy metabolism (possibly a transient stimulation by matrix $[Ca^{2+}]$ accumulation followed by inhibition as substrate uptake and PMF decrease). This pattern was not observed with the impermeant inhibitor C23 (Fig. S9).

The absence of a substantial effect of CA inhibition on ATP levels would be in agreement with energetic buffering by PCr. This energetic reserve (expressed in terms of PCr/ATP ratio) was reduced by ATZ (Fig. 4*F*), suggesting a role for CA activity in improving cardiac energetics. Interestingly, reduced energetics have been reported in skeletal muscle treated with CA inhibitors (57) or from CAIII-knockout animals (58). At constant pH_i, a down-stream effect of a decreased PCr/ATP ratio is reduced cardiac contractility (45). This was observed experimentally as the reduction of developed pressure with ATZ. Only intracellular CA isoforms participate in this effect, because the impermeant CA inhibitor C23 did not mimic the ATZ response (Fig. 4*G*). Studies on skeletal muscle have demonstrated that CA inhibitors also can affect contraction through changes to Ca^{2+} signaling. SR-associated CA activity has been proposed to accelerate the kinetics of Ca^{2+} transients by buffering $[H^+]$ changes arising from SR-membrane Ca^{2+} fluxes, thereby reducing single-twitch tension (59). This mechanism is unlikely to underlie the observed effect of ATZ on contractility. First, in perfused hearts, CA activity allowed stronger contractions. Second, the normalized rate of pressure rise was not affected by CA inhibition, suggesting that the underlying Ca^{2+} transient had not changed its time course. Indeed, studies on cardiac tissue inferred that SR-associated CA activity does not affect Ca^{2+} flux as markedly as has been demonstrated in skeletal muscle (60).

A reduced myocardial PCr/ATP ratio is characteristic of heart failure and correlates with the New York Heart Association classes of heart disease (61) and with indices of systolic (61) and diastolic (62) function and predicted prognosis (63). Off-target effects of clinically used membrane-permeant CA-inhibiting drugs (64), down-regulated CA activity, or aberrant subcellular CA distribution may lead to inefficient CO_2 venting and a mismatch between energy supply and demand and may contribute toward the heart failure phenotype. Interestingly, tachycardia-induced heart failure has been associated with reduced total CA activity (29), although whether extramitochondrial CA activity also is affected remains to be tested. Further work is warranted to explore whether the activity or size of the extramitochondrial CA domain changes in the failing heart.

Conclusions

We have shown that a cytoplasmic domain of elevated CA activity surrounds mitochondria and facilitates the venting of CO_2 generated by aerobic respiration (Fig. 4*H*). This CA-rich domain alkalinizes mitochondrial matrix pH and improves the myocardial energetic reserve. Our results demonstrate the importance of CA activity and distribution in supporting the heart's high metabolic rate. The dependence of CO_2 efflux on the subcellular distribution of CA activity exposes the system's potential to impair respiratory efficiency and contribute to the development of heart disease.

Materials and Methods

All investigations conformed to the National Institutes of Health *Guide for the Care and Use of Laboratory Animals* (65) and the UK Home Office Guidance on the Operation of the Animals (Scientific Procedures) Act, 1986.

Solutions. All chemicals, unless stated otherwise, were purchased from Sigma-Aldrich (UK). The following buffers were used (all values are in mM). KHB: NaCl (118), KCl (4.7), 1.2 $MgSO_4$ (1.2), $CaCl_2$ (1.25), KH_2PO_4 (1.2), $NaHCO_3$ (25), bubbled with 5% CO_2/95% O_2, pH 7.4 at 37 °C. Hyperpolarized ^{13}C dissolution buffer (13CB): Na_2EDTA (0.3), Tris base (20), NaOH (60), heated to 180 °C and pressurized to 10 bar. Hepes-buffered NT: KCl (4.5), glucose (11), NaCl (130), Hepes (20), $CaCl_2$ (1), $MgCl_2$ (1), pH 7.4 at 37 °C (with 4 M NaOH). CO_2/HCO_3^--buffered NT: Hepes replaced with $NaHCO_3$ (22) and solution bubbled with 5% CO_2 (balanced with air) at 37 °C (pH 7.4). Hepes-buffered IS: KCl (135), NaCl (10), Hepes (20), K-glutamate (2), K-malate (2), KH_2PO_4 (5), 2,3-butanedione monoxime (15), EGTA (5), $CaCl_2$ (2; free $[Ca^{2+}]$ = 90 nM), $MgCl_2$ (0.5), pH 7.2 at 37 °C. CO_2/HCO_3^--buffered IS: Hepes replaced with $NaHCO_3$ (14) and solution bubbled with 5% CO_2 gas (balanced with air) at 37 °C. Lysate CA assay buffer: K-gluconate (135), MgCl (1), Hepes (20), MES (20), pH 8 at 4 °C with KOH. Mitochondrial respiration buffer (MRB): KCl (35), K-Gluconate (100), K-Phosphate (1), K-ADP (0.08 or 0.3), Mg-ATP (5), K-glutamate (2), K-malate (2), Na-succinate (2), pyruvic acid (1), $NaHCO_3$ (10), EGTA (5), $MgCl_2$ (1.4), $CaCl_2$ (1.4; free $[Ca^{2+}]$ = 50 nM), bubbled with 5% CO_2/95% O_2. Mitochondrial isolation buffer (MIB): sucrose (300), EGTA (2), Tris·HCl (10), pH 7.1. Mitochondrial storage buffer (MSB): K-aspartate (100), KCl (30), KH_2PO_4 (5), K-glutamate (2), K-malate (2), NaCl (10), Hepes (10),

EGTA (5), ATP (4), $CaCl_2$ (2; free $[Ca^{2+}]$ = 90 nM), $MgCl_2$ (1), pH 7.2 at 25 °C. Mitochondrial lysis buffer (MLB): K-gluconate (100), KCl (30), $MgCl_2$ (1), Hepes (20), MES (20), pH 8. State III respiration buffer: K-gluconate (100), KCl (30), NaCl (10), K-glutamate (2), K-malate (2), KH_2PO_4 (5), ADP (0.25), EGTA (5), $MgCl_2$ (1), $CaCl_2$ (2; free $[Ca^{2+}]$ = 90 nM), pH 7.2. radioimmunoprecipitation assay (RIPA) lysis buffer: Na-deoxycholate (1g/L), Triton X-100 (1% vol/vol), NaCl (150), Tris-base (20), pH 7.3), protease inhibitor mixture. Phosphate-buffered saline (PBS) was obtained from Sigma-Aldrich. Free $[Ca^{2+}]$ was calculated using CaBuf software (G. Droogmans, Leuven, Belgium; available at ftp://ftp.cc.kuleuven.ac.be/pub/droogmans/cabuf.zip).

Superfusion. Superfusion was performed in a 1-mL Perspex chamber with a coverslip base, mounted on an inverted Zeiss Observer.Z1 microscope. Superfusate was delivered at 2 mL/min at 37 °C. A solution switcher allowed the superfusate to be changed rapidly between two lines.

Isolation of Myocytes. Myocytes were isolated following the methods in ref. 3. Myocytes from 15-wk-old Wistar hearts were isolated enzymatically with Blendzyme mixture (Roche) and stored in DMEM for use within 10 h.

Isolation of Mitochondria. Mitochondria were isolated using the methods described in ref. 39, with modifications. Hearts of 15-wk-old male Wistar rats were Langendorff-perfused with Hepes-buffered NT for 5 min to remove blood and then homogenized manually (Dounce Potter homogenizer) in ice-cold MIB containing 0.1 mg/mL protease XXIV. Tissue was centrifuged at 7,500 × *g* for 7 min at 4 °C. A sample of the pellet (labeled sample #1) was collected, washed in PBS, and lysed in RIPA for Western blotting. The remainder of the pellet was washed twice and resuspended in MIB containing protease inhibitors (Roche). The suspension was homogenized for 3 min and then centrifuged at 700 × *g* for 10 min at 4 °C. The supernatant was centrifuged at 7,000 × *g* for 10 min, and the pellet obtained was resuspended in MIB + 25% (wt/vol) Percoll. The suspension was centrifuged at 17,000 × *g* for 10 min for 4 °C, and the pellet obtained was resuspended in MIB. This suspension was centrifuged at 7,000 × *g* for 10 min at 4 °C, and the pellet was washed in MSB. A sample of this suspension was collected and labeled sample #2. The remainder was centrifuged at 7,000 × *g* for 10 min at 4 °C, and the pellet was washed in MSB. A sample of this pellet was collected and labeled sample #3. The procedure was repeated for samples #4 and #5, if required. Immunofluorescence and functional activity measurements were performed on sample #3. All samples (lysed in RIPA buffer containing protease inhibitors) were used for Western blot analysis.

Western Blotting and Immunofluorescence. PAGE and Western blotting were performed according protocols recommended for our choice of primary antibodies against LDH-B (rabbit mAb; Novus), CAII (rabbit mAb; Novus), CAXIV [rabbit polyclonal antibody (pAb); Novus], CAVA (R18, goat pAb; Santa Cruz), Mitofilin (Y17, goat pAb; Santa Cruz), RyR2 (rabbit pAb; Millipore), Serca2a (mouse mAb; Novus Biologicals). Goat anti-rabbit and anti-mouse and rabbit anti-goat secondary antibodies (Dako) and ECL (Pierce) were used to visualize the signal. Sample #3 from mitochondrial isolation was fixed in 4% (wt/wt) paraformaldehyde in PBS for 30 min (4 °C), followed by antigen blocking in 3% BSA for 30 min and with primary antibody against CAXIV (rabbit pAb, Novus) for 90 min at 37 °C. Signals were visualized with donkey anti-rabbit Alexa Fluor 555 secondary antibody.

Fluorescence Measurements. Fluorescence from suspensions of cells or mitochondria was measured using an Hitachi F4500 cuvette spectrofluorometer at 25 °C. Fluorescence imaging of isolated cells or mitochondria was performed on a Zeiss LSM700 confocal microscope, integrated with a superfusion system, at 37 °C. A 40× oil-immersion objective was used for fluorescence pH measurements. For immunofluorescence and colocalization experiments, a 100× objective was used instead. Flow cytometry was performed on a Beckman Coulter SC Quanta (25 °C). See *SI Materials and Methods* for dye-loading procedures and wavelength settings.

Hyperpolarized ^{13}C MRS. Hyperpolarized [1-^{13}C]pyruvate was prepared and administered, and ^{13}C spectra were acquired as described previously (30–32) and in *SI Materials and Methods*. For in vivo imaging, a ^{13}C pulse-acquire MRS sequence was used in an intact, ~300-g male Wistar rat with a surface coil on its chest [the heart is the dominant source of PDH activity in the chest (32)]. Hyperpolarized [1-^{13}C]pyruvate (80 μmol) was infused i.v. over 10 s, and 30 spectra were acquired over 1 min. Metabolism of this substrate to $^{13}CO_2$ occurs exclusively in the matrix by pyruvate dehydrogenase (37). Experiments were repeated on rats infused with 2 μmol of the membrane-impermeant CA inhibitor C23 (38), 25 μmol of the membrane-permeant CA inhibitor ATZ, or 25 μmol DIDS to block HCO_3^- exchange between red cells and plasma, each dissolved in 1 mL saline and injected 15 min before [1-^{13}C]pyruvate. Assuming C23 retention in the extracellular space (20% of 300 g) and ATZ distribution in the total body water (60% of 300 g), concentrations of drugs would exceed their inhibitory constants over the MRS time frame (C23 K_i = 14 μM, ATZ K_i = 53 nM; Fig. S2). ^{13}C MR spectra were analyzed as described in *SI Materials and Methods*. Ex vivo measurements were performed on excised rat hearts that were Langendorff perfused with KHB containing [1-^{13}C]pyruvate, as described previously (31, 66) and in *SI Materials and Methods*.

$H^{13}CO_3^-$ Quenching. Hearts were perfused in Langendorff mode with KHB containing [1-^{13}C]pyruvate, and metabolically generated $^{13}CO_2$ and $H^{13}CO_3^-$ were detected using ^{13}C MRS with 1-s temporal resolution for 2 min. At 20-s intervals during ^{13}C spectral acquisition, radio-frequency saturation was applied to the $H^{13}CO_3^-$ resonance to quench the $H^{13}CO_3^-$ signal using a cascade of eight SNEEZE pulses (*SI Materials and Methods*).

Cardiac Energetics and Contractile Function. Hearts were Langendorff perfused with KHB, and ^{31}P spectra were acquired to measure the PCr, P_i, and γ-ATP resonances as described in *SI Materials and Methods*. Cytoplasmic pH was calculated from the P_i chemical shift (67). Contractile function was measured by the insertion into the left ventricle of a water-filled balloon attached to a pressure transducer. Contractility was monitored in each heart perfused with the following for 40 min each: (*i*) perfusion buffer, (*ii*) buffer with 35 μM C23, and (*iii*) buffer with 35 μM C23 and 100 μM ATZ. Contractile function was reported as the average DP over the final 10 min of each perfusion series.

ACKNOWLEDGMENTS. We thank Ms. Mala Rohling and Mr. Philip Cobden for excellent technical support with isolating cardiac myocytes and Dr. Robert Wilkins for access to the cuvette spectrofluorometer. This work was supported by the Wellcome Trust (M.A.S.), International Society of Heart Research (M.A.S.), British Heart Foundation Grants RG/07/004/22659 (to K.C.), RG/08/016 (to R.D.V.-J.), and FS/10/002/28078 (to D.J.T.), the Medical Research Council (P.S.), and the Royal Society (P.S.). D.J.T. and K.C. received research support from GE Healthcare.

1. Väänänen HK, Carter ND, Dodgson SJ (1991) Immunocytochemical localization of mitochondrial carbonic anhydrase in rat tissues. *J Histochem Cytochem* 39(4):451–459.
2. Scheibe RJ, et al. (2006) Expression of membrane-bound carbonic anhydrases IV, IX, and XIV in the mouse heart. *J Histochem Cytochem* 54(12):1379–1391.
3. Leem CH, Vaughan-Jones RD (1998) Out-of-equilibrium pH transients in the guinea-pig ventricular myocyte. *J Physiol* 509(Pt 2):471–485.
4. Morgan PE, Pastoreková S, Stuart-Tilley AK, Alper SL, Casey JR (2007) Interactions of transmembrane carbonic anhydrase, CAIX, with bicarbonate transporters. *Am J Physiol Cell Physiol* 293(2):C738–C748.
5. Alvarez BV, Vilas GL, Casey JR (2005) Metabolon disruption: A mechanism that regulates bicarbonate transport. *EMBO J* 24(14):2499–2511.
6. Sterling D, Reithmeier RA, Casey JR (2001) A transport metabolon. Functional interaction of carbonic anhydrase II and chloride/bicarbonate exchangers. *J Biol Chem* 276(51):47886–47894.
7. Boron WF (2010) Evaluating the role of carbonic anhydrases in the transport of HCO_3^- related species. *Biochim Biophys Acta* 1804(2):410–421.
8. Nakayama S, Sakuyama T, Mitaku S, Ohta Y (2002) Fluorescence imaging of metabolic responses in single mitochondria. *Biochem Biophys Res Commun* 290(1):23–28.
9. Duchen MR, Leyssens A, Crompton M (1998) Transient mitochondrial depolarizations reflect focal sarcoplasmic reticular calcium release in single rat cardiomyocytes. *J Cell Biol* 142(4):975–988.
10. Kettlewell S, et al. (2009) Changes of intra-mitochondrial Ca^{2+} in adult ventricular cardiomyocytes examined using a novel fluorescent Ca^{2+} indicator targeted to mitochondria. *J Mol Cell Cardiol* 46(6):891–901.
11. Maack C, et al. (2006) Elevated cytosolic Na^+ decreases mitochondrial Ca^{2+} uptake during excitation-contraction coupling and impairs energetic adaptation in cardiac myocytes. *Circ Res* 99(2):172–182.
12. Kurz FT, Aon MA, O'Rourke B, Armoundas AA (2010) Spatio-temporal oscillations of individual mitochondria in cardiac myocytes reveal modulation of synchronized mitochondrial clusters. *Proc Natl Acad Sci USA* 107(32):14315–14320.
13. Aon MA, Cortassa S, Marbán E, O'Rourke B (2003) Synchronized whole cell oscillations in mitochondrial metabolism triggered by a local release of reactive oxygen species in cardiac myocytes. *J Biol Chem* 278(45):44735–44744.
14. Cannon PJ, Dell RB, Dwyer EM, Jr. (1972) Measurement of regional myocardial perfusion in man with 133 xenon and a scintillation camera. *J Clin Invest* 51(4): 964–977.
15. Ashikawa K, Kanatsuka H, Suzuki T, Takishima T (1986) Phasic blood flow velocity pattern in epimyocardial microvessels in the beating canine left ventricle. *Circ Res* 59(6):704–711.
16. Kawashiro T, Scheid P (1976) Measurement of Krogh's diffusion constant of CO_2 in respiring muscle at various CO_2 levels: Evidence for facilitated diffusion. *Pflugers Arch* 362(2):127–133.

17. Gros G, Moll W (1971) The diffusion of carbon dioxide in erythrocytes and hemoglobin solutions. *Pflugers Arch* 324(3):249–266.
18. Uchida K, Mochizuki M, Niizeki K (1983) Diffusion coefficients of CO_2 molecule and bicarbonate ion in hemoglobin solution measured by fluorescence technique. *Jpn J Physiol* 33(4):619–634.
19. Engel J, Fechner M, Sowerby AJ, Finch SA, Stier A (1994) Anisotropic propagation of Ca^{2+} waves in isolated cardiomyocytes. *Biophys J* 66(6):1756–1762.
20. Vendelin M, Birkedal R (2008) Anisotropic diffusion of fluorescently labeled ATP in rat cardiomyocytes determined by raster image correlation spectroscopy. *Am J Physiol Cell Physiol* 295(5):C1302–C1315.
21. Elder JA, Lehninger AL (1973) Respiration-dependent transport of carbon dioxide into rat liver mitochondria. *Biochemistry* 12(5):976–982.
22. Waisbren SJ, Geibel JP, Modlin IM, Boron WF (1994) Unusual permeability properties of gastric gland cells. *Nature* 368(6469):332–335.
23. Musa-Aziz R, Chen LM, Pelletier MF, Boron WF (2009) Relative CO_2/NH_3 selectivities of AQP1, AQP4, AQP5, AmtB, and RhAG. *Proc Natl Acad Sci USA* 106(13):5406–5411.
24. Geers C, Gros G (2000) Carbon dioxide transport and carbonic anhydrase in blood and muscle. *Physiol Rev* 80(2):681–715.
25. Vandenberg JI, et al. (1996) Carbonic anhydrase and cardiac pH regulation. *Am J Physiol* 271(6 Pt 1):C1838–C1846.
26. Dodgson SJ, Forster RE, 2nd, Storey BT, Mela L (1980) Mitochondrial carbonic anhydrase. *Proc Natl Acad Sci USA* 77(9):5562–5566.
27. Santo-Domingo J, Demaurex N (2012) Perspectives on: SGP symposium on mitochondrial physiology and medicine: The renaissance of mitochondrial pH. *J Gen Physiol* 139(6):415–423.
28. Alvarez BV, et al. (2007) Carbonic anhydrase inhibition prevents and reverts cardiomyocyte hypertrophy. *J Physiol* 579(Pt 1):127–145.
29. Dzeja PP, Pucar D, Redfield MM, Burnett JC, Terzic A (1999) Reduced activity of enzymes coupling ATP-generating with ATP-consuming processes in the failing myocardium. *Mol Cell Biochem* 201(1-2):33–40.
30. Ardenkjaer-Larsen JH, et al. (2003) Increase in signal-to-noise ratio of > 10,000 times in liquid-state NMR. *Proc Natl Acad Sci USA* 100(18):10158–10163.
31. Schroeder MA, et al. (2010) Measuring intracellular pH in the heart using hyperpolarized carbon dioxide and bicarbonate: A ^{13}C and ^{31}P magnetic resonance spectroscopy study. *Cardiovasc Res* 86(1):82–91.
32. Schroeder MA, et al. (2008) In vivo assessment of pyruvate dehydrogenase flux in the heart using hyperpolarized carbon-13 magnetic resonance. *Proc Natl Acad Sci USA* 105(33):12051–12056.
33. Storey BT, Lin LC, Tompkins B, Forster RE, 2nd (1989) Carbonic anhydrase in guinea pig skeletal muscle mitochondria. *Arch Biochem Biophys* 270(1):144–152.
34. Swietach P, et al. (2008) Tumor-associated carbonic anhydrase 9 spatially coordinates intracellular pH in three-dimensional multicellular growths. *J Biol Chem* 283(29): 20473–20483.
35. Forster RE, 2nd (1991) Methods for the measurement of carbonic anhydrase activity. *The Carbonic Anhydrases: Cellular Physiology and Molecular Genetics*, ed Dodgson SJ (Plenum, New York).
36. Itada N, Forster RE (1977) Carbonic anhydrase activity in intact red blood cells measured with ^{18}O exchange. *J Biol Chem* 252(11):3881–3890.
37. Merritt ME, et al. (2007) Hyperpolarized ^{13}C allows a direct measure of flux through a single enzyme-catalyzed step by NMR. *Proc Natl Acad Sci USA* 104(50):19773–19777.
38. Svastová E, et al. (2004) Hypoxia activates the capacity of tumor-associated carbonic anhydrase IX to acidify extracellular pH. *FEBS Lett* 577(3):439–445.
39. Bednarczyk P, Barker GD, Halestrap AP (2008) Determination of the rate of $K(^+)$ movement through potassium channels in isolated rat heart and liver mitochondria. *Biochim Biophys Acta* 1777(6):540–548.
40. Inui M, Wang S, Saito A, Fleischer S (1988) Characterization of junctional and longitudinal sarcoplasmic reticulum from heart muscle. *J Biol Chem* 263(22): 10843–10850.
41. Unitt JF, Schrader J, Brunotte F, Radda GK, Seymour AM (1992) Determination of free creatine and phosphocreatine concentrations in the isolated perfused rat heart by ^1H- and ^{31}P-NMR. *Biochim Biophys Acta* 1133(2):115–120.
42. Xiong JW, Zhu L, Jiao X, Liu SS (2010) Evidence for DeltapH surface component (DeltapH(S)) of proton motive force in ATP synthesis of mitochondria. *Biochim Biophys Acta* 1800(3):213–222.
43. Silverman HS, et al. (1994) Regulation of intracellular free Mg^{2+} and contraction in single adult mammalian cardiac myocytes. *Am J Physiol* 266(1 Pt 1):C222–C233.
44. Sato K, et al. (1995) Insulin, ketone bodies, and mitochondrial energy transduction. *FASEB J* 9(8):651–658.
45. Dos Santos P, et al. (2000) Metabolic control of contractile performance in isolated perfused rat heart. Analysis of experimental data by reaction:diffusion mathematical model. *J Mol Cell Cardiol* 32(9):1703–1734.
46. Dorn GW, 2nd, Scorrano L (2010) Two close, too close: Sarcoplasmic reticulum-mitochondrial crosstalk and cardiomyocyte fate. *Circ Res* 107(6):689–699.
47. Rizzuto R, et al. (2009) $Ca(^{2+})$ transfer from the ER to mitochondria: When, how and why. *Biochim Biophys Acta* 1787(11):1342–1351.
48. Shah GN, et al. (2005) Carbonic anhydrase IV and XIV knockout mice: Roles of the respective carbonic anhydrases in buffering the extracellular space in brain. *Proc Natl Acad Sci USA* 102(46):16771–16776.
49. Hallerdei J, et al. (2010) T tubules and surface membranes provide equally effective pathways of carbonic anhydrase-facilitated lactic acid transport in skeletal muscle. *PLoS ONE* 5(12):e15137.
50. Vargas LA, Alvarez BV (2012) Carbonic anhydrase XIV in the normal and hypertrophic myocardium. *J Mol Cell Cardiol* 52(3):741–752.
51. Kifor G, Toon MR, Janoshazi A, Solomon AK (1993) Interaction between red cell membrane band 3 and cytosolic carbonic anhydrase. *J Membr Biol* 134(3):169–179.
52. Liu T, O'Rourke B (2008) Enhancing mitochondrial Ca^{2+} uptake in myocytes from failing hearts restores energy supply and demand matching. *Circ Res* 103(3):279–288.
53. Griffiths EJ, Rutter GA (2009) Mitochondrial calcium as a key regulator of mitochondrial ATP production in mammalian cells. *Biochim Biophys Acta* 1787(11): 1324–1333.
54. Shah GN, et al. (2000) Mitochondrial carbonic anhydrase CA VB: Differences in tissue distribution and pattern of evolution from those of CA VA suggest distinct physiological roles. *Proc Natl Acad Sci USA* 97(4):1677–1682.
55. Poburko D, Santo-Domingo J, Demaurex N (2011) Dynamic regulation of the mitochondrial proton gradient during cytosolic calcium elevations. *J Biol Chem* 286(13):11672–11684.
56. Vaughan-Jones RD, Spitzer KW, Swietach P (2009) Intracellular pH regulation in heart. *J Mol Cell Cardiol* 46(3):318–331.
57. Geers C, Gros G (1990) Effects of carbonic anhydrase inhibitors on contraction, intracellular pH and energy-rich phosphates of rat skeletal muscle. *J Physiol* 423: 279–297.
58. Liu M, Walter GA, Pathare NC, Forster RE, Vandenborne K (2007) A quantitative study of bioenergetics in skeletal muscle lacking carbonic anhydrase III using ^{31}P magnetic resonance spectroscopy. *Proc Natl Acad Sci USA* 104(1):371–376.
59. Wetzel P, Kleinke T, Papadopoulos S, Gros G (2002) Inhibition of muscle carbonic anhydrase slows the $Ca(^{2+})$ transient in rat skeletal muscle fibers. *Am J Physiol Cell Physiol* 283(4):C1242–C1253.
60. Geers C, Gros G (1995) Contractile function of papillary muscles with carbonic anhydrase inhibitors. *Life Sci* 57(6):591–597.
61. Neubauer S, et al. (1992) ^{31}P magnetic resonance spectroscopy in dilated cardiomyopathy and coronary artery disease. Altered cardiac high-energy phosphate metabolism in heart failure. *Circulation* 86(6):1810–1818.
62. Lamb HJ, et al. (1999) Diastolic dysfunction in hypertensive heart disease is associated with altered myocardial metabolism. *Circulation* 99(17):2261–2267.
63. Neubauer S, et al. (1997) Myocardial phosphocreatine-to-ATP ratio is a predictor of mortality in patients with dilated cardiomyopathy. *Circulation* 96(7):2190–2196.
64. Aggarwal M, McKenna R (2012) Update on carbonic anhydrase inhibitors: A patent review (2008 - 2011). *Expert Opin Ther Pat* 22(8):903–915.
65. Committee on Care and Use of Laboratory Animals (1985) *Guide for the Care and Use of Laboratory Animals* (Natl Inst Health, Bethesda) DHEW (NIH) Publ No 85–23, revised 1996.
66. Schroeder MA, et al. (2012) The cycling of acetyl-coenzyme A through acetylcarnitine buffers cardiac substrate supply: A hyperpolarized ^{13}C magnetic resonance study. *Circ Cardiovas Imaging* 5(2):201–209.
67. Bailey IA, Williams SR, Radda GK, Gadian DG (1981) Activity of phosphorylase in total global ischaemia in the rat heart. A phosphorus-31 nuclear-magnetic-resonance study. *Biochem J* 196(1):171–178.